Involvement of Electrostatic Interactions in the Mechanism of Peptide Folding Induced by Sodium Dodecyl Sulfate Binding † , ‡

ARTICLE *in* BIOCHEMISTRY · AUGUST 2000

Impact Factor: 3.02 · DOI: 10.1021/bi000208x · Source: PubMed

Articles

Involvement of Electrostatic Interactions in the Mechanism of Peptide Folding Induced by Sodium Dodecyl Sulfate Binding[†,‡]

Roland Montserret,[§] Michael J. McLeish,[||,⊥] Anja Böckmann,[§] Christophe Geourjon,[§] and François Penin*[,§]

Institut de Biologie et de Chimie des Protéines, CNRS UPR 412, 7 passage du Vercors, 69367 Lyon Cedex 07, France, and Victorian College of Pharmacy, Monash University, 381 Royal Pde, Parkvillle 3052, Australia

Received February 1, 2000; Revised Manuscript Received May 8, 2000

ABSTRACT: Sodium dodecyl sulfate (SDS) has consistently been shown to induce secondary structure, particularly α-helices, in polypeptides, and is commonly used to model membrane and other hydrophobic environments. However, the precise mechanism by which SDS induces these conformational changes remains unclear. To examine the role of electrostatic interactions in this mechanism, we have designed two hydrophilic, charged amphipathic α-helical peptides, one basic (QAPAYKKAAKKLAES) and the other acidic (QAPAYEEAAEELAKS), and their structures were studied by CD and NMR. The design of the peptides is based on the sequence of the segment of residues 56−70 of human platelet factor 4 [PF4-(56−70), QAPLYKKIIKKLLES]. Both peptides were unstructured in water, and in the presence of neutral, zwitterionic, or cationic detergents. However, in SDS at neutral pH, the basic peptide folded into an α-helix. By contrast, the pH needed to be lowered to 1.8 before α-helix formation was observed for the acidic peptide. Strong, attractive electrostatic interactions, between the anionic groups of SDS and the cationic groups of the lysines, appeared to be necessary to initiate the folding of the basic peptide. NMR analysis showed that the basic peptide was fully embedded in SDS−peptide micelles, and that its three-dimensional α-helical structure could be superimposed on that of the native structure of PF4(56−70). These results enabled us to propose a working model of the basic peptide−SDS complex, and a mechanism for SDS-induced α-helical folding. This study demonstrates that, while the folding of peptides is mostly driven by hydrophobic effects, electrostatic interactions play a significant role in the formation and the stabilization of SDS-induced structure.

Sodium dodecyl sulfate (SDS)[1] is an amphipathic anionic molecule which is widely employed in protein biochemistry for its powerful dissociation and solubilization properties (for an overview, see refs *1* and *2*). Since the addition of SDS to proteins invariably leads to the loss of their biological activity, it is often mistakenly believed that SDS completely unfolds proteins, a belief perpetuated by SDS−PAGE protocols. In fact, SDS has, for a long time, been shown to induce and stabilize secondary structure, particularly α-helices (*3*−*5*). Consequently, SDS micelles have been used extensively for the structural investigations of membrane peptides, as they provide an anionic, membrane-mimicking environment with a hydrophobic core and a polar head (*6*−*10*). Moreover, because of its ability to induce and stabilize ordered conformations in peptides having structure-forming potential (*5*, *11*), SDS is often used along with TFE for probing the conformation of small protein fragments such as folding initiation sites (*12*−*15*) or unfolded protein regions involved in recognition processes (*16*; for an overview about TFE, see refs *16* and *17*).

Micellar SDS is known to stabilize an α-helical conformation in peptides derived from helical regions of the original

[†] This work was supported by the Centre National de la Recherche Scientifique, by the Association pour la Recherche sur le Cancer (ARC, Grant 1178 to F.P.), by a Program Emergence grant from the Région Rhône-Alpes (France), and by the Monash Research Fund (Australia).

[‡] The coordinates of the average structures and the NMR restraints have been deposited with the Brookhaven Protein Data Bank under accession codes 1DJF for the basic peptide in 50% TFE, 1DN3 for the basic peptide in 40 mM SDS, and 1DNG for the acidic peptide in 50% TFE. The corresponding proton and carbon chemical shifts of the assigned residues have been deposited in the BioMagResBank (BMRB) under accession numbers 4723 and 4724 for the acidic and basic peptides, respectively.

* To whom correspondence should be addressed. E-mail: f.penin@ibcp.fr. Fax: 334 72 72 26 01.

[§] Institut de Biologie et de Chimie des Protéines.

[||] Monash University.

[⊥] Present address: College of Pharmacy, The University of Michigan, Ann Arbor, MI 48109.

[1] Abbreviations: 2D and 3D, two- and three-dimensional, respectively; CD, circular dichroism; cmc, critical micellar concentration; DQF-COSY, double-quantum-filtered correlation spectroscopy; HSQC, heteronuclear single-quantum coherence; NOE, nuclear Overhauser enhancement; NOESY, nuclear Overhauser enhancement spectroscopy; NMR, nuclear magnetic resonance; rmsd, root-mean-square deviation; ROESY, rotating frame Overhauser effect spectroscopy; RP-HPLC, reversed-phase high-performance liquid chromatography; SDS, sodium dodecyl sulfate; TFE, 2,2,2-trifluoroethanol; TOCSY, total correlation spectroscopy; TSP-d_4, 3-(trimethysilyl)propionic-2,2,3,3-d_4 acid; WATERGATE, water suppression by gradient-tailored excitation.

10.1021/bi000208x CCC: $19.00
Published on Web 00/00/0000

protein (*5*, *12*−*14*, *18*, *19*). Moreover, peptides derived from regions of β-sheet (*15*, *20*) as well as peptides predicted to be β-strand (*21*) could also form stable helices in micellar SDS. However, at concentrations below its CMC (1−10 mM depending on the ionic strength; see ref *22*), SDS has been shown to promote β-strand structure in the latter peptides (*15*, *20*, *21*), as well as β-strand structure in peptides with helical propensity (*20*, *23*).

At present, the molecular mechanism by which micellar and/or nonmicellar SDS acts to induce and/or stabilize secondary structure in peptides is unclear. For hydrophobic membrane peptides, it is generally reported that peptides penetrate deeply into the hydrophobic core of the SDS micelles and adopt an α-helical structure due to hydrophobic interactions (*6*, *7*). For amphipathic peptides, SDS micelles provide a hydrophobic environment, presumably allowing the folding and stabilization to be driven by hydrophobic effects (*5*, *18*−*21*). However, the crystallographic studies of lysozyme (*24*) have shown clearly that the sulfate group of SDS forms stable salt bridges with positively charged amino acids. Such electrostatic interactions can play an important role in the formation and/or stability of the SDS-induced conformation of peptides. Indeed, Wu and co-workers (*5*, *23*) suggested that anionic groups of SDS first bind to the cationic groups of a polypeptide while additional SDS molecules cluster around the polypeptide chain to induce an ordered structure. By contrast, anionic Glu and Asp residues can destabilize the SDS-induced peptide conformation if they are located in the structure-forming segments (*23*). Given the fact that electrostatic interactions can be an essential driving force for α-helix or β-sheet formation in some biorecognition processes (such as interactions between the anionic groups of heparin and the cationic groups of heparin-binding peptides; *25*−*27*), consideration should be given to the thought that similar processes might occur upon formation of SDS−peptide mixed micelles. In addition, electrostatic SDS−peptide interactions also raise the question of the localization of charged peptides relative to SDS micelle; i.e., is the peptide anchored via electrostatic bonds at the surface of the micelle as suggested by some studies (for example, see ref *28*), or is it incorporated into the hydrophobic core of the micelle?

Further understanding of the role of electrostatic versus hydrophobic interactions in the process of SDS-inducing peptide conformation would be aided by the three-dimensional structural analysis of SDS−polypeptide complexes. Toward this goal, we have designed two hydrophilic amphipathic peptides, based on the sequence of the segment of residues 56−70 of human platelet factor 4 (PF4; *29*) and analyzed their α-helical folding propensity in various environments by circular dichroism (CD) and NMR spectroscopy. The PF4(56−70) segment (i.e., QAPLYKKIIKKLLES) is a basic amphipathic α-helix, and its four lysine residues play an essential role in the binding of the peptide to the negatively charged groups of heparin (*30*). We report here the 3D structures of both designed peptides in 50% TFE and that of the basic peptide in 40 mM SDS. Detailed NMR analyses have allowed us to display a working model of the SDS−basic peptide complex and to propose a mechanism for SDS binding and induction of α-helical folding. This provides us with molecular insights into the role of electrostatic interactions in the mechanism of SDS-inducing peptide conformation and into the SDS−polypeptide interaction process, in general.

EXPERIMENTAL PROCEDURES

Sodium dodecyl-d_{25} sulfate (SDS-d_{25}, >98% isotopic enrichment) was purchased from Isotech Inc., while 2,2,2-trifluoroethyl-1,1-d_2 alcohol (TFE-d_2, >99% isotopic enrichment) was from Euriso-Top. SDS, Triton X-100, dodecyl β-D-maltoside, Chaps, dodecyltrimethylammonium bromide, 1-dodecanesulfonic acid, and routine chemicals were from Sigma. C12E8 was obtained from Calbiochem.

Peptide Synthesis. Both peptides were synthesized using the stepwise solid-phase method of Merrifield and employing Fmoc (9-fluorenylmethyloxycarbonyl) chemistry, in a Millipore 9050 plus continuous flow synthesizer. For each peptide, the C-terminal carboxylate group was synthesized in the amide form, while the N-terminal amide group was acetylated with acetic anhydride. This was done to suppress the charged N- and C-terminal groups and to give a greater degree of similarity to the longer peptide. After removal of protecting groups and cleavage from the resin with TFA, the crude product was lyophilized before purification by preparative RP-HPLC on a Vydac C18 column using 0.1% aqueous trifluoroacetic acid and an acetonitrile gradient. The resulting peptides appeared as a single peak on analytical RP-HPLC and exhibited the expected molecular mass, as measured by electrospray mass spectrometry (1646 and 1649 Da for the basic and acidic peptides, respectively). Peptide concentrations were determined by UV absorbance of tyrosine using a molar extinction coefficient of 1536 M^{-1} cm^{-1} at 280 nm and neutral pH.

Circular Dichroism Measurements. CD spectra were recorded on either a Jobin-Yvon CD6 or a Jasco J-710 spectrometer equipped with variable-temperature units and calibrated with ammonium *d*-10-camphorsulfonate. Routinely, measurements were carried out at 298 K in 0.1 cm path length quartz cuvettes (Hellma) with peptide concentrations ranging from 20 to 110 μM in 10 mM sodium phosphate buffer (pH 7.4). Spectra were recorded in the 190−250 nm wavelength range with 0.2 nm increments and an integration time of 2 s. The baseline-corrected spectra were smoothed by using a third-order least-squares polynomial fit. Assuming that the residue molar ellipticity at 222 nm is exclusively due to α-helix (*31*), we estimated the α-helical content using the following equation: % helix = $100[\theta]_{obs\lambda}/[\theta]_{H\lambda}$, where $[\theta]_{obs\lambda}$ is the observed mean residue ellipticity and $[\theta]_{H\lambda}$ is the maximum mean residue ellipticity for a helix of finite length. $[\theta]_{H\lambda}$ was calculated using the empirical equation for helix length dependence proposed by Chen et al. (*32*): $[\theta]_{H\lambda} = [\theta]_{H\lambda\infty}(f_H - ik/N)$, where $[\theta]_{H\lambda\infty}$ is the maximum mean residue ellipticity for a helix of infinite length (−39500 for $\lambda = 222$ nm), f_H is the fraction of helix, i is the number of helical segments (1 in this case), k is a wavelength-dependent constant (2.57 for $\lambda = 222$ nm), and N is the number of residues.

NMR Spectroscopy. Lyophilized samples were dissolved in a mixture of aqueous sodium phosphate buffer containing either 50% TFE-d_2 or 40 mM SDS-d_{25}. TSP-d_4 was added as an internal reference in all samples. For H−D exchange experiments, the lyophilized SDS−basic peptide sample

(previously adjusted to pH 4.0 with HCl) was solubilized in 100% D_2O and NMR spectra were recorded at appropriate time intervals over the course of 24 h. All NMR experiments were carried out at 500 MHz on a Varian Unity-*plus* spectrometer equipped with *ultra-nmr* shims and using a triple-resonance proton−carbon−nitrogen 5 mm probe with a self-shielded z gradient coil. Spectra were acquired nonspinning at temperatures ranging from 283 to 333 K. Two-dimensional (2D) homonuclear ^{1}H experiments (DQF-COSY, Clean-TOCSY, NOESY, and ROESY) and ^{13}C−^{1}H experiments (gHSQC and gHSQC-TOCSY) were performed using conventional pulse sequences. All data collection and processing were carried out as described in detail previously (*33*, *34*). For NOESY experiments, mixing times in the 50−300 ms range were used to evaluate spin diffusion. Water suppression was carried out using selective, low-power irradiation during the 1.5 s relaxation delay, and during the mixing time in NOESY experiments. Alternatively, water was suppressed using a WATERGATE sequence prior to detection. The resonances of protons were ascribed by the conventional assignment method (*35*). In short, spin systems were identified using DQF-COSY and TOCSY spectra, with the help of ^{13}C−^{1}H HSQC and HSQC-TOCSY spectra at various temperatures (283, 293, and 303 K), to resolve the overlap of resonances. Sequential assignments were performed on the basis of NOESY spectra recorded at mixing times of 150 and 300 ms.

NMR-Derived Constraints and Structure Calculations. NOE intensities used as input for the structure calculations were obtained from the NOESY spectrum recorded with a 300 ms mixing time and checked for spin diffusion with spectra recorded at shorter mixing times (50−150 ms). NOEs were partitioned into three categories of intensities that corresponded to distances ranging from a common lower limit of 1.8 Å to upper limits of 2.6, 3.8, and 5 Å, for strong, medium, and weak intensities, respectively. The cross-peak intensities of the H^{δ}−H^{ϵ} protons of Tyr5 were used as the distance reference (2.45 Å). Dihedral angles Φ were constrained between 0 and −60° each time, the $^3J_{NH\alpha}$ coupling constants were less than 5.5 Hz. Protons without stereospecific assignments were treated as pseudoatoms, and the correction factors were added to the upper and lower distance constraints (*35*). NOE back-calculations were performed from calculated structures using the standard procedure contained in X-PLOR 3.1 (*36*).

Three-dimensional (3D) structures were generated from NOE distances with X-PLOR 3.1 (*36*) using the standard force fields and default parameter sets, except for some minor modifications, used as described previously (*34*), to increase the duration of the molecular dynamic simulations and the number of energy minimization steps. Sets of 50 structures were calculated to widely sample the conformational space, and the structures were analyzed for NOE and dihedral angle violations. The selected structures were compared via their pairwise rmsds over the backbone atom coordinates (N, Cα, and C′). Statistical analysis, superimposition of structures, 3D graphic display, and manipulations were carried out using either ANTHEPROT 2.6 (*37*) or RASMOL 2.5 (*38*). The secondary structure elements and Ramachandran plots were analyzed according to the Kabsch−Sander definition rules, as incorporated into PROCHECK-NMR (*39*).

RESULTS

Peptide Design. Preliminary experiments with the chemically synthesized peptide, QAPLYKKIIKKLLES, corresponding to the segment of residues 56−70 of human platelet factor 4 [named PF4(56−70)], showed that it was essentially unfolded in aqueous solution, as also reported previously (*40*), but adopted an α-helical conformation upon binding to heparin. This indicates that electrostatic interactions between the cationic groups of PF4(56−70) and the sulfate and carboxylate groups of heparin provide an essential driving force for at least the initiation of α-helical folding (F. Penin and M. J. McLeish, unpublished data). Similarly, PF4(56−70) also folded into an α-helix upon addition of SDS micelles, suggesting that a similar mechanism might be in use. However, the SDS−PF4(56−70) complex yielded poorly resolved NMR spectra whose cross-peaks were too broad to be exhaustively analyzed for 3D structure determination. Moreover, PF4(56−70) is a rather hydrophobic amphipathic peptide which tended to aggregate in nonmicellar SDS, and therefore did not provide all the features necessary for a good model to clearly define the role of electrostatic interactions in SDS−peptide complex formation and α-helical folding. Consequently, it was decided to prepare a more hydrophilic peptide, in which most of the Ile and Leu residues of PF4(56−70) were replaced with Ala residues. In this manner, the hydrophobicity of the peptide was decreased (hydrophobicity indexes of 0.73, 0.53, and 0.25 for Ile, Leu, and Ala, respectively; *41*) but the propensity of the peptide to fold into an α-helix was maintained (helicity parameters of 1.08, 1.21, and 1.42 for Ile, Leu, and Ala, respectively; *42*). In the resulting "basic" peptide, QAPAYKKAAKKLAES, the Leu residue at position 12 was conserved for NMR assignment purposes. Indeed, it proved to be essential for structure reconstruction to be able to unambiguously distinguish between the lysine residues at positions 7 and 11 thanks to their NOE correlations with different $i + 1$ neighboring residues. Another peptide, QAPAYEEAAEELAKS, denoted the "acidic" peptide, was designed to study the repulsive electrostatic effects in SDS−peptide complexes. This peptide was derived from the basic peptide by converting all lysine residues to glutamic acid residues, and with the original Glu at position 14 being replaced with a Lys.

Circular Dichroism Analyses. The CD spectrum of the basic peptide in aqueous solution at pH 7.4 exhibits a single negative band at 198 nm (Figure 1A) typical of a peptide in a random coil conformation (*31*). Upon addition of TFE, the spectrum changes with the appearance of two minima at 207 and 222 nm, and a maximum at 192 nm. This process took place while the TFE concentration increased from 0 to 40% (v/v). An isodichroic point was observed at 204 nm, indicating that the peptide undergoes a simple random coil to α-helix transition and, according to a two-state model, that an equilibrium exists between the two conformers (*43*). Increasing the TFE concentration from 40 to 50% TFE resulted in only minor changes in the amplitude of the spectrum (Figure 1A), and no further modification was observed above 50% TFE (data not shown). This is consistent with the suggestion of Jasanoff and Fersht (*44*) that, for a peptide with high helical propensity, the helicity is generally at a maximum by 20−30% TFE and complete by 50%. The

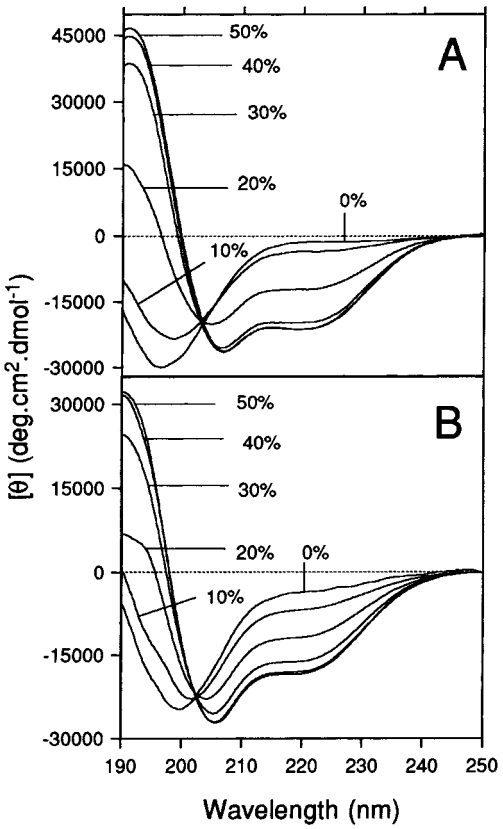

FIGURE 1: Far-UV CD spectra of (A) the basic peptide and (B) the acidic peptide at the indicated TFE concentration (v/v). The peptide concentrations were 24.9 and 24.7 μM, respectively, in 10 mM sodium phosphate buffer at pH 7.4 and 293 K.

maximal molecular ellipticity observed at 222 nm corresponded to an α-helical content of 64%. Similar behavior was observed for the acidic peptide upon addition of TFE (Figure 1B); i.e., the CD spectra were characteristic of coil to α-helix transition, with an isodichroic point at 203 nm. Again, the maximal molecular ellipticity at 222 nm was reached by 40% TFE, and the corresponding helical content was estimated to be 56%. These data demonstrate that both the basic and acidic peptides exhibit a similar propensity to fold into α-helix upon addition of TFE.

In the presence of SDS at pH 7.4, the basic peptide appears to behave in the same way as in TFE (Figure 2A). Below 0.25 mM SDS, it remains in a random coil conformation with a negative band at 198 nm. Between 0.25 and 2 mM SDS, it undergoes a simple random coil to α-helix transition as evidenced by the appearance of a double minimum at 208 and 222 nm, a positive band at 193 nm, and an isodichroic point at 204 nm. Between 2 and 10 mM SDS (and even up to 200 mM, not shown), no change in the shape or in the amplitude of maxima and minima was observed, and a maximum helical content of 52% was calculated. Hence, the SDS-dependent folding of the basic peptide is complete by 2 mM SDS, a concentration which is below the critical micellar concentration (cmc) of SDS in the buffer used in this study (7−10 mM; *22*). This suggests that the peptide lowers the cmc of SDS due to the formation of a mixed peptide−SDS micelle (*45*). In contrast, at pH 11.0, where the α-amino groups of the lysine residues are deprotonated, the SDS concentration must be raised to at least 10 mM (i.e., above its cmc) to reach the maximum amplitude of SDS-induced α-helical folding of the basic peptide (data not shown). Together, these results indicate that, at neutral pH, a strong interaction occurs between the SDS molecules and the peptide which is presumably due to the primary electrostatic binding of the sulfate groups of SDS molecules to the α-amino groups of the lysines (*23*).

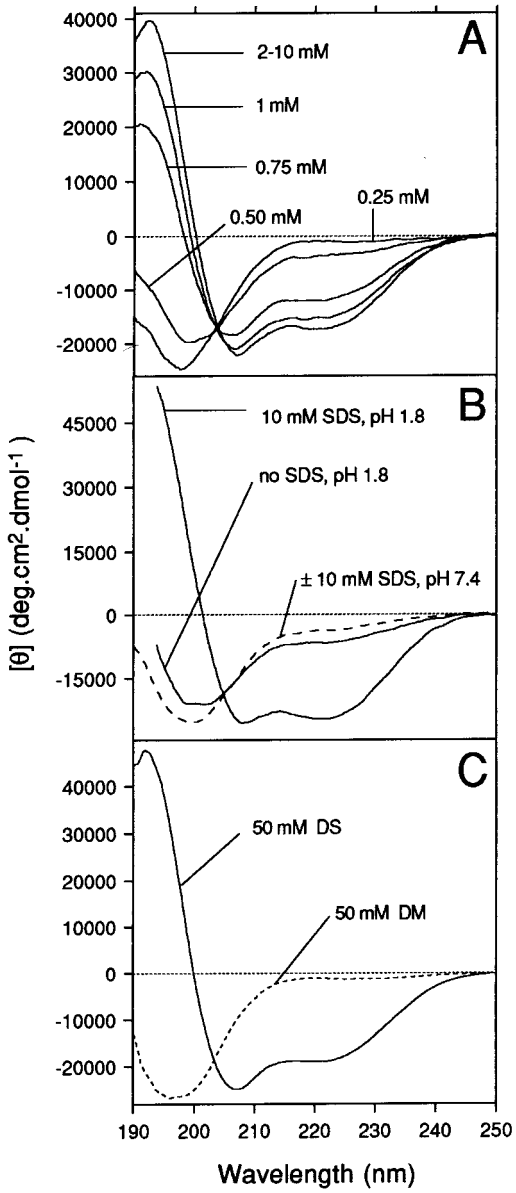

FIGURE 2: Effect of SDS on the conformation of the basic and acidic peptides monitored by far-UV CD at 293 K. (A) SDS titration of the basic peptide at 24.9 μM in 10 mM sodium phosphate buffer (pH 7.4). (B) Effect of SDS on the acidic peptide (24.7 μM) at pH 7.4 (dotted line, no SDS; dashed line, 10 mM SDS) and pH <1.8 (solid line, SDS concentration as indicated) in 10 mM sodium phosphate buffer.

Unlike the behavior observed for the basic peptide, the acidic peptide did not fold into α-helix upon addition of SDS at neutral pH (pH 7.4, Figure 2B), no matter what SDS concentration was used (up to 200 mM). However, at 10 mM SDS and at a pH of <1.8, the CD spectrum of the acidic peptide displayed the characteristic double minimum at 208 and 222 nm for the helical conformation (Figure 2B). This SDS-dependent helix formation reached its maximum at 10 mM SDS, which is around the cmc of SDS under the buffer conditions that were used (*22*). These findings clearly

indicate that protonation of the carboxylic acid groups of glutamic acid side chains is necessary to avoid electrostatic repulsion and permits helix formation brought about by hydrophobic interactions between uncharged residues and the SDS hydrophobic tail. Further, these data demonstrate that repulsive electrostatic interactions between the anionic amino acid groups and the sulfate groups of SDS are able to completely prevent SDS-induced α-helix formation in the acidic peptide.

In addition to SDS, several other detergents have been tested for their ability to induce the structure in both the basic and acidic peptides. However, neither the neutral (dodecyl β-D-maltoside, C12E8, and Triton X-100) nor the zwitterionic (Chaps) detergents that were examined, at concentrations ranging from 0.1 to 100 mM, showed any measurable effect on the conformation of either peptide (see Figure 2C for dodecyl β-D-maltoside; data not shown for the other detergents). This indicates that the hydrophobic interactions between these detergents and the peptides are, in themselves, not sufficient to promote an α-helical conformation for either peptide. This is true even for detergents having a 12-carbon hydrophobic tail such as dodecyl β-D-maltoside, i.e., a hydrophobic potential similar to that of SDS. Further, and contrary to what may have been be expected on the basis of potential electrostatic interactions, the cationic detergent dodecyltrimethylamonium bromide was not able to induce folding of the acidic peptide. This is possibly due to the lower strength of the carbonyl−amide salt bridge when compared to that of the sulfate−amide salt bridge. In addition, the cationic detergent had no effect on the basic peptide conformation, and in fact, among the various detergents tested to date, only 1-dodecanesulfonic acid was able to induce an α-helical folding which is comparable to that observed with SDS (Figure 2C). Taken together, these results indicate that the attractive electrostatic interaction of sulfate or sulfonate groups with the positively charged peptide residues plays a major role in the induction and stabilization of the detergent-dependent helical conformation of the basic peptide.

NMR Spectroscopy. During the optimization of the NMR sample conditions, it was found that, for a 10 mM basic peptide solution, a concentration of only 40 mM SDS-d_{25} was required to ensure full α-helical folding of the peptide. This was checked by the absence of amide proton chemical shift variation while increasing the SDS concentration up to 200 mM. Interestingly, this peptide:SDS ratio corresponds to a stoichiometry of four SDS molecules per peptide, and given the presence of four Lys residues in the basic peptide, it may be inferred that α-helix formation is linked to the attractive electrostatic binding of SDS to Lys residues. Nonetheless, this indicates that the helical structure is brought about by formation of a mixed peptide micelle. Figure 3 shows extracts of the NOESY spectra corresponding to the fingerprint region (NH−αH,βH) and the amide region (NH−NH) of the basic peptide in 50% TFE (panels A and B of Figure 3, respectively) and in 40% SDS (panels C and D of Figure 3, respectively). Figure 4 shows the corresponding NOESY extracts for the acidic peptide in 50% TFE. For each peptide, the resonances were ascribed to individual protons in a sequence-specific manner by the conventional assignment method (*35*). The ^{1}H and ^{13}C chemical shifts for both peptides in water and 50% TFE and for the basic peptide in 40 mM SDS are available at the BioMagResBank (BMRB access numbers 4723 and 4724).

In the presence of 50% TFE, the backbone amide region of NOESY spectra of both peptides (Figures 3B and 4B) exhibited strong NH−NH cross-peaks, and the corresponding fingerprint region (Figures 3A and 4A) showed that sequential NOE cross-peaks [i.e., dαN(i,i+1) connectivities] were stronger than the corresponding intraresidual cross-peaks. This is typical for peptides folded into a predominantly α-helical conformation. The good spectral resolution allowed the straightforward assignment of all spin systems (Figures 3 and 4). In the basic peptide, Pro3 appeared to be in only the trans conformation, as deduced by the strong cross-peak between the Ala2 αH and the Pro3 δH. By contrast, in the acidic peptide while Pro3 was mostly in the trans conformation, about 10% of the peptide population appeared to adopt a cis conformation. Moreover, at 283 K, the sequential assigment of the cis isomer of Pro3 could be carried out from Ala2 to Ala8 (data not shown). Apart from the small population of cis conformers observed for the acidic peptide, no evidence for any other stable conformation was found for either peptide. The NOESY spectra also showed that, for both peptides, the backbone amide proton of Gln1 and the aromatic protons of Tyr5 displayed poorly resolved cross-peaks (Figures 3A and 4A), indicating substantial flexibility in the N-terminus of the peptides and in the aromatic side chain of Tyr5.

NOESY spectra of the basic peptide in SDS micelles (panels C and D of Figure 3) showed much broader resonances than the spectra of the peptide in TFE, but were sufficiently well-resolved to allow the assignment of all spin systems. The backbone amide region (Figure 3D) displayed good peak dispersion (with the exception of the overlap of Lys7 and Lys11) and exhibited strong NOE amide cross-peaks indicative of helical folding. In addition, this region also showed that the ring protons of Tyr5 were well-resolved, and numerous cross-peaks with amide protons could be observed. Moreover, the number of Tyr5 aromatic to aliphatic cross-peaks in the fingerprint region (Figure 3C) clearly indicates that the conformation of this aromatic ring is much less flexible in the presence of SDS than is observed in the presence of TFE (panels A and B of Figure 3).

Secondary Structure. Figure 5 shows the sequences of the basic and acidic peptides with an overview of sequential and medium-range NOE connectivities obtained from NOESY experiments and $^3J_{NHH\alpha}$ coupling constants for the basic peptide in 50% TFE and 40 mM SDS (panels A and B of Figure 5, respectively) and for the acidic peptide in 50% TFE (Figure 5C).

The analysis of NOEs of the basic peptide in 50% TFE (Figure 5A) shows that connectivities, characteristic of α-helical conformation, are observed from Tyr5 to Ala13. These include strong dNN(i,i+1) and medium dαN(i,i+1) sequential connectivities and numerous medium dαN(i,i+3), strong dαβ(i,i+3), and weak dαN(i,i+4) medium-range connectivities. In addition, the $^3J_{NHH\alpha}$ coupling constants measured along the sequence were 5.5 Hz, typical of an α-helical conformation. The exceptions were the constants for Gln1, Glu14, and Ser15, residues located in the termini of the peptide, where $^3J_{NHH\alpha}$ coupling constants between 5.5 and 8 Hz were observed. Taken together, these data demonstrate that the segment between Tyr5 and Ala13 adopted an α-helical conformation. The C-terminal region

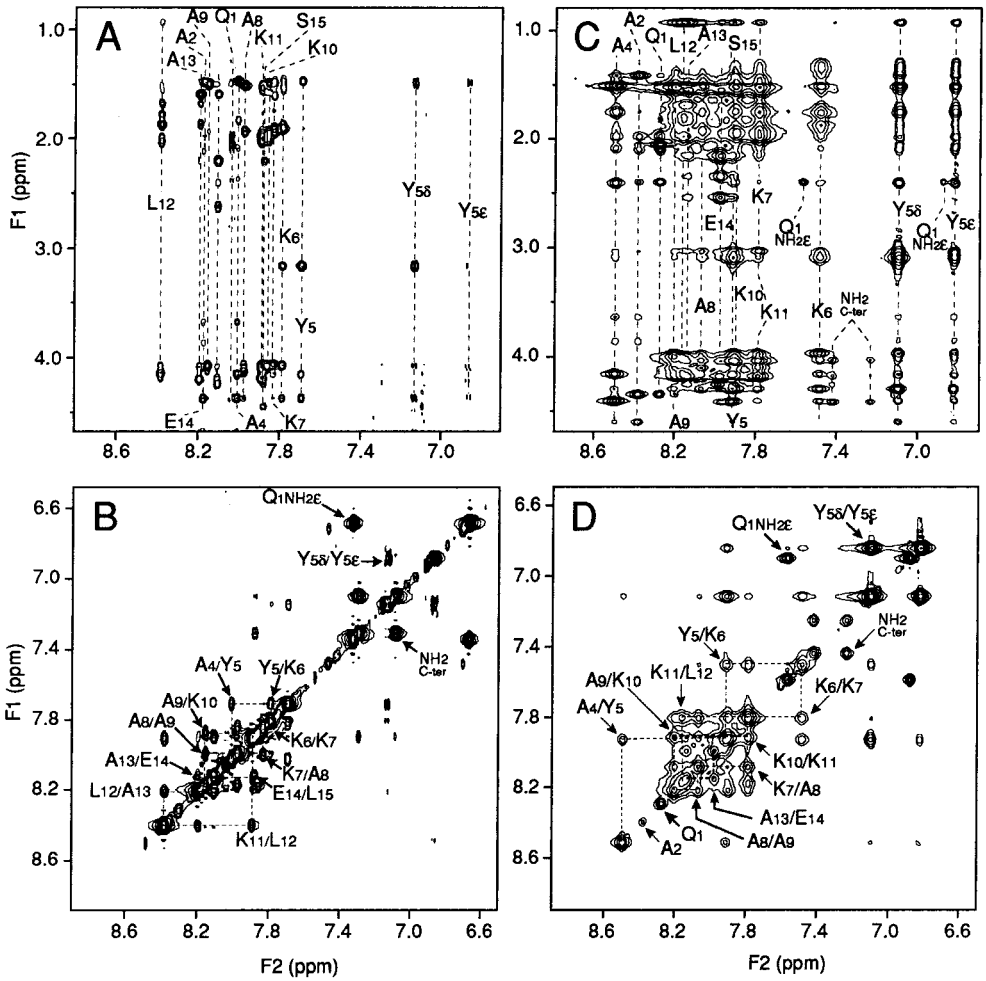

FIGURE 3: Extracts of NOESY spectra of the basic peptide in 50% TFE (A and B) and in 40 mM SDS (C and D). Peptide concentrations were 10.4 and 11 mM for TFE and SDS samples, respectively, in 10 mM sodium phosphate buffer (pH 6.0). NOESY spectra were recorded at 293 K with a mixing time of 150 ms. (A and C) NH−aliphatic region, where the cross-peaks between each NH and its through-space neighboring protons are indicated with a dotted line. (B and D) NH−NH region, where sequencial resonance assignments are traced out and intraresidual side chain protons are indicated.

of the basic peptide (Glu14 and Ser15) also exhibited some sequential and medium-range NOE connectivities, indicative of helical conformers, but the high $^3J_{NHH\alpha}$ coupling constants indicate that this region is probably flexible. For the N-terminal region of the peptide (Gln1−Ala4), despite the low values of $^3J_{NHH\alpha}$ observed for Ala2 and Ala4, the lack of NN(i,i+1) NOEs and medium-range connectivities indicate that this region is unstructured.

For the basic peptide in 40 mM SDS (Figure 4B), resonance broadening meant that no $^3J_{NHH\alpha}$ coupling constants could be measured. Nevertheless, there is strong evidence that this peptide forms an α-helix, with numerous dαN(i,i+3), dαβ(i,i+3), and dαN(i,i+4) medium-range connectivities being observed for the residues between Ala4 and Ser15. Further confirmation was obtained from a ^{13}C and ^{1}H chemical shift index analysis [CSI (*46*); data not shown]. Therefore, as observed in 50% TFE, the basic peptide in SDS clearly adopts an α-helical conformation between Ala4 and Ala13. Again, the N-terminal region of the peptide does not show any medium-range NOEs, indicating the absence of any stable folded conformers in this region. Finally, these data show that the overall conformation of the basic peptide is very similar in both 50% TFE and 40 mM SDS.

The pattern of NOE connectivities and $^3J_{NHH\alpha}$ coupling constants observed for the Ala4−Ala13 segment of the acidic peptide in 50% TFE (Figure 4C) was also quite similar to that observed for the basic peptide with (i) strong dNN(i,i+1) and medium dαN(i,i+1) sequential NOE connectivities, (ii) medium dαN(i,i+3), strong dαβ(i,i+3), and weak dαN(i,i+4) medium-range NOE connectivities, and (iii) a $^3J_{NHH\alpha}$ of 5.5 Hz. These data show that the Ala4−Ala13 region of the acidic peptide also adopts an α-helical conformation. As with the basic peptide, the N- and C-termini of the acidic peptide appear to be flexible as evidenced by the low number of NOE connectivities, and $^3J_{NHH\alpha}$ coupling constant values in the 5.5−8.0 Hz range. Overall, these results indicate that the backbone structure of the acidic peptide in 50% TFE is very similar to that observed for the basic peptide.

Structure Calculations and 3D Structure Analysis. For both peptides in 50% TFE, a set of distance constraints was first defined using the NOESY spectrum at 293 K, and completed with new constraints identified from NOESY spectra recorded at 283 and 303 K. The slight temperature-dependent chemical shift changes in the amide region were enough to resolve cross-peak overlaps, without changing the overall conformation of the peptide. This strategy allowed us to obtain a set of constraints sufficient for molecular modeling

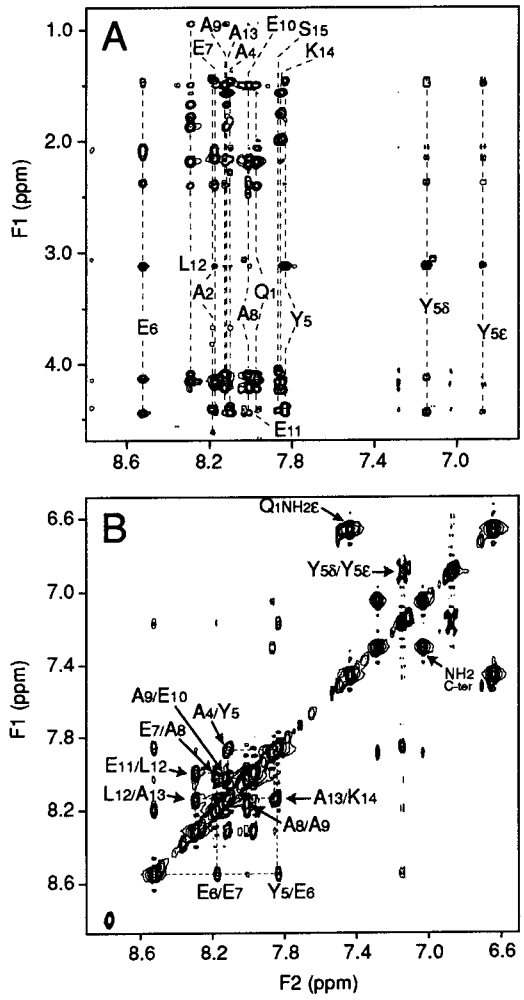

FIGURE 4: Extract of NOESY spectra of the acidic peptide in 50% TFE. The peptide (11.2 mM) was in 10 mM sodium phosphate buffer (pH 6.0). NOESY spectra were recorded at 293 K with a mixing time of 200 ms. (A) NH−aliphatic region, where the cross-peaks between each NH and its through-space neighboring protons are indicated with a dotted line. (B) NH−NH region, where sequencial resonance assignments are traced out and intraresidual side chain protons are indicated.

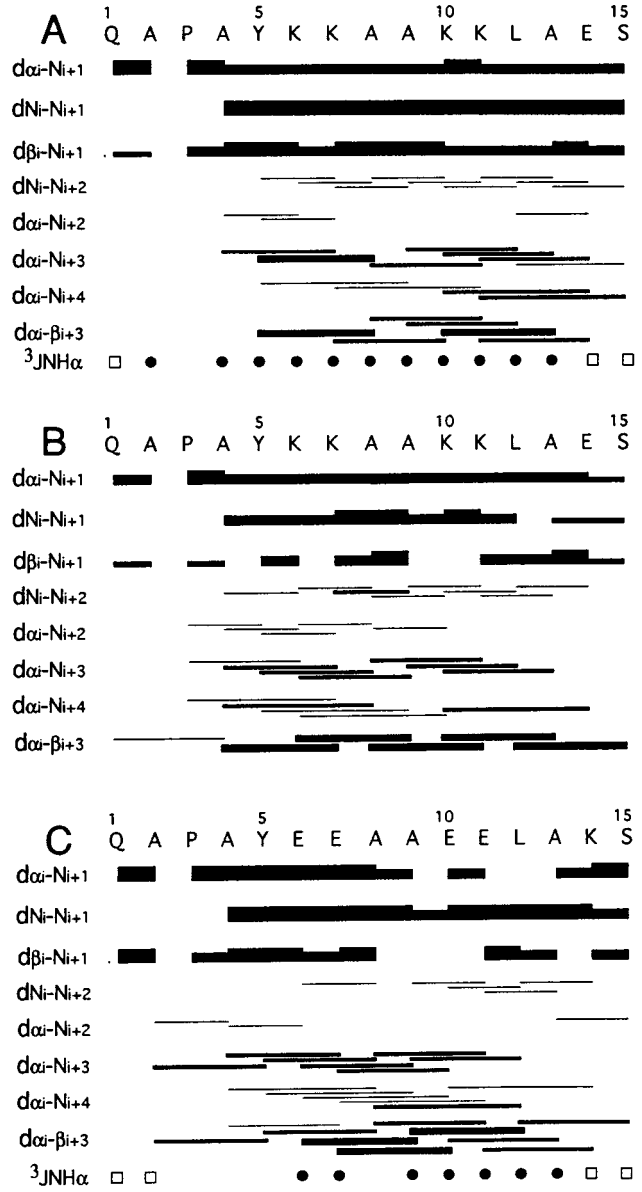

FIGURE 5: Summary of sequential (*i*,*i*+1) and medium-range (*i*,*i*+2 to *i*,*i*+4) NOEs and $^3J_{NHH\alpha}$ coupling constants for (A) the basic peptide in 50% TFE, (B) the basic peptide in 40 mM SDS, and (C) the acidic peptide in 50% TFE. Intensities of NOEs are indicated by the heights of the bars. Coupling constants were measured on one-dimensional spectra: (●) $^3J_{NHH\alpha} = 5.5$ Hz and (□) $5.5 < {}^3J_{NHH\alpha} < 8$ Hz.

(summarized in Table 1). As no dihedral constraints were available for the basic peptide in SDS, 82 intraresidual constraints were added in the molecular modeling process performed with X-PLOR 3.1 (*36*). No additional H-bonds were introduced into the calculations despite the clear indications of α-helical folding. From the initial 50 structures calculated in each case, a final set of structures was selected on the basis of the absence of both NOE violations of 0.5 Å, and dihedral constraint violations of 5°. The structures selected in this manner correspond to those structures exhibiting the lowest energy among the 50 structures that were generated. The overall energy of the selected structures is quite negative, with values of less than −50 kcal mol^{-1} for both peptides in TFE, and less than −40 kcal mol^{-1} for the basic peptide in SDS. In summary, all the selected structures fully satisfied the experimental NMR data.

Figure 6 shows the superposition of the final set of calculated structures for the basic peptide in either 50% TFE (32 structures, Figure 6A) or 40 mM SDS (38 structures, Figure 6B), and for the acidic peptide in 50% TFE (40 structures, Figure 6C). In all cases, the N-terminal region appeared to be disordered while the Tyr5−Ala13 segments were very well defined, with rms deviations of less than 0.37 Å for the backbone heavy atoms (C′, Cα, and N), and less than 1.72 Å when all atoms are taken into account (Table 1). The backbone dihedral angles indicated only few deviations from ideal covalent geometry, with more than 95% of the residues being located in the allowed regions of the Ramachandran plots (Table 1). These data, and the pairwise rmsd analysis, exemplified the good convergence of the calculated structures, and indicated the presence of only one family of structures in each case. As expected, the distribution of charged versus nonpolar residues in each structure clearly showed the amphipathic character of the helices.

The average NMR structures calculated for the basic peptide, in either 50% TFE or 40 mM SDS, and for the acidic peptide in 50% TFE were compared to that of PF4(46−70)

Table 1: Statistics on the Final Sets of Simulated Annealing Structures[a]

	basic peptide in 50% TFE	basic peptide in 40 mM SDS	acidic peptide in 50% TFE
(A) Constraints			
no. of distance restraints			
intraresidue	0	82	0
sequential	83	96	95
medium-range	43	99	125
total	126	277	220
no. of dihedral angle constraints			
Φ angles	10	0	8
(B) Statistics for the Final X-PLOR Structures			
no. of structures in the final set	32	38	40
X-PLOR energy (kcal mol^{-1})	-56.7 ± 7.8	-40.6 ± 8.6	-68.9 ± 8.8
NOE violations			
no. >0.5 Å	none	none	none
rmsd (Å)	0.05 ± 0.009	0.05 ± 0.008	0.07 ± 0.004
dihedral violations			
no. >5°	none		none
rmsd (deg)	0.2 ± 0.3		0.04 ± 0.18
deviation from idealized covalent geometry			
angles (deg)	1.1 ± 0.07	1.3 ± 0.09	0.12 ± 0.07
impropers (deg)	0.22 ± 0.02	0.28 ± 0.03	0.27 ± 0.02
bonds (Å)	0.005 ± 0.0002	0.005 ± 0.0003	0.005 ± 0.0002
rmsd (Å)			
backbone (C′, Cα, and N)			
helix (residues 5−13)	0.32	0.37	0.33
all residues	1.86	1.89	1.48
all heavy atoms			
helix (residues 5−13)	1.72	1.62	1.37
all residues	2.91	2.78	2.40
Ramachandran data[b]			
residues in most favored regions (%)	90.9	87.3	80.0
residues in allowed regions (%)	6.8	8.1	19.2
residues in generously allowed regions (%)	2.3	2.4	0.8
residues in disallowed regions (%)	0	2.2	0

[a] See Experimental Procedures for details of calculation. [b] From PROCHECK-NMR (*39*).

(Figure 6D) deduced from crystallographic data (*30*). The superposition of these structures guided by their common α-helix, and the fact that the Cα pairwise RMSD was less than 0.5 Å for any pair of structures (data not shown), clearly demonstrate the close similarity of the individual helices. This shows that, in the presence of stabilizing cosolvents, the acidic and basic peptides both adopt an helical conformation which mimics the native fold of the corresponding PF4-(56−70) segment from which they are derived.

Interactions between the Basic Peptide and SDS. To obtain more information about the exact positioning of the basic peptide in the peptide−SDS complex, the water accessibility of the individual amide hydrogen atoms was checked by monitoring their exchange behavior with water. As the exchange is too rapid at pH 6.0 to be observed with D_2O isotope methods, the relative rate of exchange was estimated by using exchange spectroscopy selective at the water frequency as described previously (*47*). The data (not shown) indicated that the exchange rates were on the millisecond time scale and were rather uniform along the peptide chain. However, higher signal intensities observed for residues Gln1, Ala2, and Ser15 gave some evidence for faster exchange in the termini of the peptide. It should be noted that no observations were made for the amide protons of Tyr5 and Lys10, as they were superimposed with that of the Ser15 amide proton (which could be unambiguously identified by the cross signals of its α- and β-protons in a 2D water selective NOESY control experiment). These results were confirmed and complemented by the H−D exchange NMR experiments carried out at lower pH (pH 4.0). These showed that the half-lives for amide proton exchange were less than 1 min for Gln1, in the 10−20 min range for Ala2, Ala4, Glu14, and Ser15, and in the range of 4−8 h for the residues of the Tyr5−Ala13 segment. Unfortunately, the signals of Ala9, Leu12, and Ala13 were overlapped at pH 4.0, and their exchange rates could not be individually measured. However, in general, the slowly exchanging amide protons belonged to those residues situated in the well-defined α-helix, while the rapidly exchanging protons were located in the flexible N- and C-terminal regions. For residues Ala9−Ala13, the slow exchange rates could be explained by the involvement of their amide protons in the α-helix hydrogen bond network. Yet, as the amide protons of the first four residues of an α-helix are not involved in this network, this does not explain the slow exchange rates of the Tyr5, Lys6, Lys7, and Ala8 amide protons. It is not unreasonable to postulate that these slow exchange rates are brought about by the embedding of those residues in the SDS−peptide complex. This is supported by a detailed examination of the line widths of resonances of the basic peptide in SDS (panels C and D of Figure 3). These show that the cross-peaks involving residues from Lys6 to Ala13 are much broader than those for Gln1, Ala2, and Ala4, indicating much faster motions for the latter. In summary, these data suggest that the Tyr5−Ala13 segment is embedded in a hydrophobic environment within the SDS−peptide complex, whereas termini are exposed at the SDS−peptide complex interface and/or in the aqueous solution.

To observe direct contact between SDS and the basic peptide atoms, NOESY spectra were measured in the

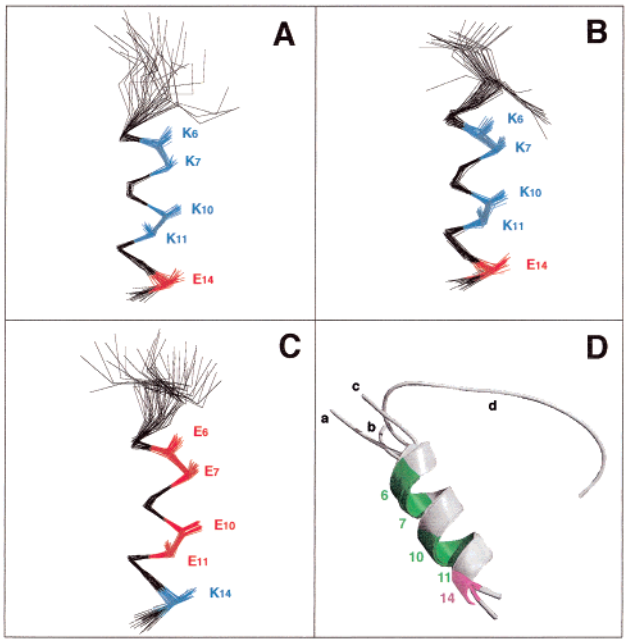

FIGURE 6: NMR structures of the basic and acidic peptides and comparison with the PF4(46−70) X-ray structure. (A) Superimposition of the final set of 32 structures of the basic peptide in 50% TFE. (B) Superimposition of the final set of 38 structures of the basic peptide in 40 mM SDS. (C) Superimposition of the final set of 40 structures of the acidic peptide in 50% TFE. (D) Superimposition of the average structures of the basic peptide in 50% TFE (a) and in 40 mM SDS (b) with the average structure of the acidic peptide in 50% TFE (c) and the average crystallographic structure (d) of human platelet factor 4 (residues 46−70) deduced from Zhang et al. (*30*) (PDB entries 1DJF, 1DN3, 1DNG, and 1RHP for a−d, respectively). The α-carbons of each set of structures were superimposed from residue 5 to 13 [from 60 to 68 for PF4(46−70)] with ANTHEPROT software tools (*37*). The Cα−Cβ bonds of the indicated charged residues are represented. The basic and acid residues are colored in blue and red, respectively, except in panel D where residues 6, 7, 10, and 11 are in green and residue 14 is in purple (see the text for explanation). Panels A−C were rendered with RASMOL (*38*). Panel D was generated with MOLSCRIPT (*52*) and rendered with RASTER 3D (*53*).

presence of a 1:3 ratio of protiated SDS/SDS-d_{25} (*48*). A significant number of intermolecular NOEs cross-peaks were observed (Figure 7). These included SDS C1H, C2H, and C3H with the ϵCH_2 of lysine residues, with the δCH_3 and $\delta' CH_3$ of Leu12, and with the δCH and ϵCH of Tyr5; and SDS $(CH_2)_n$ with the same and with the αH and βCH_2 of Tyr5, with the αHs of Lys6, Leu12, and Ala13, and with the NHs of Ala4, Tyr5, Lys6, Ala8, Lys10, and Leu12. From this, it appears that almost all the residues in the α-helical region of the basic peptide provide intermolecular cross-peaks with SDS. Conversely, no cross-peaks were observed arising from the N- and C-terminal residues. These data also suggest that the whole α-helix is embedding in the SDS−peptide complex. Remarkably, the cross-peak intensities between the SDS C1H and the ϵCH_2 of lysine residues are greater than those observed with the δCH_3 and $\delta' CH_3$ of Leu12, or with the δCH and ϵCH of Tyr5. This is true even if the intensities of the four overlapping ϵCH_2 of the lysines are actually compared to the 2 × 3 methyl protons of Leu12, or the 2 × 2 ring protons of Tyr5. By contrast, the intensities of the cross-peaks between SDS C2H and methyl protons of Leu12 are much greater than those observed with the ϵCH_2 of lysine. These cross-peak comparisons, and others, indicate that the anionic head of SDS preferentially interacts with the cationic group of the lysine residues, while the hydrophobic tail of SDS preferentially interacts with the hydrophobic methylene and methyl groups of peptide residues. These results (i) support the formation of salt bridges between the anionic head of SDS molecules and the cationic group of lysines and (ii) provide evidence for the positioning of the SDS molecules relative to the residues of the peptide α-helix.

DISCUSSION

We have designed two very hydrophilic amphipathic peptides, one basic and the other acidic, and have shown that both peptides are unfolded in water. In 50% TFE, they adopted the same α-helical structure as the corresponding region of the 3D crystal structure of PF4(56−70), the region from which they are derived. This demonstrates that their intrinsic α-helical folding propensity was conserved despite the amino acid substitutions made to increase the hydrophilicity of the peptide, and regardless of whether the side chain residues were predominantly negatively or positively charged. Thus, these peptides constitute very good models for studying the role of electrostatic interactions in the mechanism of SDS-induced α-helical folding.

Neither the basic nor the acidic peptide was seen to adopt a folded conformation in the presence of neutral, zwitterionic, or cationic detergents, even those having a C_{12} hydrophobic tail similar to that of SDS. This indicates that the hydrophobic interactions between peptide and detergent hydrophobic tails are not sufficient, in themselves, to create a stable hydrophobic core that would promote the α-helical folding of these peptides. Furthermore, SDS-induced α-helical folding of the acidic peptide was not observed above pH 1.8. Presumably, this indicates that the carboxyl group needed to be protonated for folding to occur and, therefore, that repulsive electrostatic interactions can prevent the formation of a stable SDS−peptide complex, a finding in accord with those of Wu et al. (*23*). By contrast, SDS induced the α-helical folding of the basic peptide at any pH via a simple and smooth random coil to α-helix transition, and SDS−peptide interaction lowered the cmc of SDS probably because of the formation of mixed peptide−SDS micelles. These results suggest that the strong attractive electrostatic interactions between the anionic polar heads groups of SDS and cationic groups of lysine are necessary to initiate this folding process. In addition, the SDS−peptide interaction gives rise to a 3D structure in which the α-helical region can be superimposed on that of the native structure of PF4(56−70), and on that obtained for the peptide in 50% TFE. These data are in agreement with the current view that SDS can induce helical structure in peptide segments that have α-helix-forming potential (*20*, *21*, *23*).

Although the SDS−basic peptide NMR analysis yielded valuable information about the direct proton contacts between both compounds, it is unfortunately not possible to accurately determine the position of the SDS molecules in the SDS−peptide complex. However, to summarize and visualize the SDS−basic peptide interaction features reported above, a schematic molecular working model has been drawn and is displayed in Figure 8. The SDS molecules were positioned onto the average 3D structure of the basic peptide taking into account (i) the formation of salt bridges between the

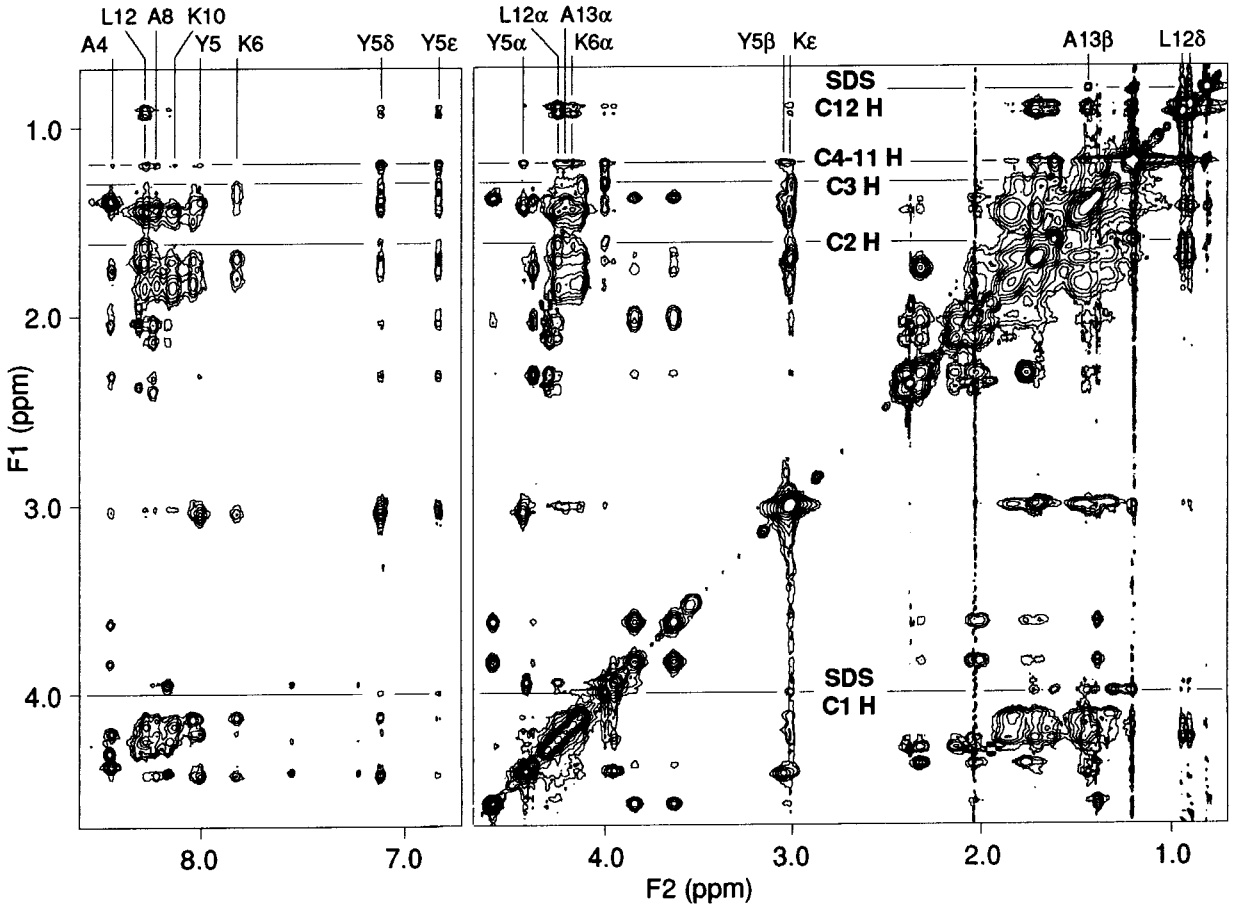

FIGURE 7: Portion of the NOESY spectrum of the basic peptide in the presence of a 3:1 SDS-d_{25}/SDS mixture at pH 6.0 and 293 K. The peptide:SDS molar ratio was 1:4 (10 and 40 mM, respectively). Selected NOE cross-peaks between SDS and the basic peptide are labeled.

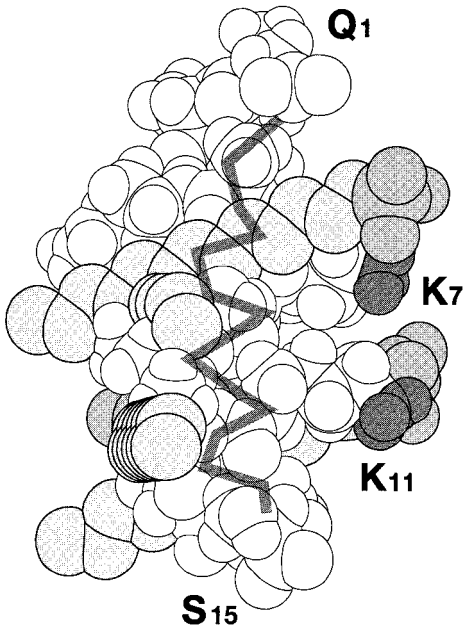

FIGURE 8: Schematic molecular representation of basic peptide−SDS complex. SDS molecules were built using PRO-EXPLORE (Oxford Molecular Ltd.) and manually positioned with the basic peptide average structure (see the text). The sulfate groups and the aliphatic tails of SDS are colored dark gray and light gray, respectively. The cationic groups of Lys7 and Lys11 are colored black. The peptide backbone is colored dark gray.

amino group of lysine residues and the sulfate groups of SDS molecules, (ii) the direct contacts established by the observation of NOEs between the individual peptide residues and the aliphatic tails of SDS, (iii) the minimum stoichiometry of four SDS molecules per peptide molecule (1:1 SDS:lysine ratio) shown to be sufficient for attaining the complete α-helical folding at high peptide and SDS concentrations (10 and 40 mM, respectively), and (iv) the noninvolvement of the peptide termini in the SDS−peptide complex. These features give rise to an amphipathic peptide−SDS complex with sulfate groups of SDS and cationic lysine side chains on the same side, while SDS tails and nonpolar peptide residues are located on the opposite, hydrophobic side.

It should be noted that, regardless of the model displayed in Figure 8, there is no formal evidence for the positioning of SDS perpendicular to the α-helical axis. This position was chosen because it fit better to the extended side chains of lysine residues, and because it highlights the size of the SDS hydrophobic tail relative to the width of the α-helix. Although these four SDS tails clearly should not be as rigid as portrayed in Figure 8, it can be see that they are long enough to wrap around the helix from one side to the other. It is likely that some reorganization must take place to ensure the maximum number of close hydrophobic contacts between SDS tails, the hydrophobic part of lysine side chains, and the other nonpolar groups of the peptide. This will yield a more compact and thus more stable complex. However, as suggested by the quite rapid exchange rate of the peptide amide protons at pH 6.0, the hydrophobic contacts likely fluctuate rapidly. Finally, the broad NMR signals indicate that this 4:1 SDS−basic peptide complex probably does not

exist as a monomer in solution. It is reasonable to suggest that it forms large peptide−SDS mixed micelles containing several peptide molecules, organized around a central hydrophobic core made of the α-helix hydrophobic side of peptide−SDS complexes, and surrounded by the α-helix hydrophilic (SDS−lysine salt bridges) side of these complexes. Nevertheless, although the basic peptide is very hydrophilic, its whole α-helical region appears to be fully embedded in the mixed micelles.

Although this working model is only approximate, it constitutes a reasonable molecular basis for better understanding how SDS can induce the folding of the basic peptide. In the first step, the sulfate groups of SDS likely bind to the cationic groups of lysine (*23*, *49*). We think that these strong salt bridges (*24*) act as anchors, allowing the CH_2 groups of the SDS tail to associate with hydrophobic residues. The general accommodation of all hydrophobic groups will create a hydrophobic cluster by the exclusion of water. This process leads to the stabilization of peptide intramolecular hydrogen bonds, to the detriment of any intermolecular hydrogen bonding with water. Hence, as the peptide possesses an intrinsic propensity to form an α-helix, it adopts a stable α-helical folding through the formation of the α-helix hydrogen bond network.

Consequently, it appears that, in toto, the SDS-induced folding is driven by hydrophobic interactions, which is in line with current thoughts about the formation of local secondary structure (*43*, *50*, *51*). However, it should be pointed out that electrostatics do play a role, as it appears that the initial formation of SDS−lysine salt bridges may initiate the α-helical folding process by anchoring the anionic group head of SDS to the basic peptide. Indeed, in the absence of such an electrostatic anchor, it appears that the binding of hydrophobic C_{12} tails of other detergents are not able to form a stable peptide−detergent complex allowing the formation of a hydrophobic environment required for α-helix hydrogen bond network stabilization. The present proposed mechanism highlights the essential role of amino acid side chains, both charged and hydrophobic, in the sequential cooperative process of the SDS-induced mechanism of α-helix formation.

In conclusion, one can wonder whether this mechanism can be generalized to other peptides possessing a propensity to form α-helix. SDS is a bifunctional molecule, able to bind by both hydrophobic and charge interactions (*20*), and as a rule, its binding should be viewed as a cooperative process involving both interactions. For highly hydrophilic, amphipathic α-helical peptides, such those studied here, it is clear that interaction between SDS and the charged residues is essential for determining whether folding will be initiated. Conversely, for very hydrophobic peptides such as transmembrane peptide segments, the SDS−peptide hydrophobic interactions may be sufficiently strong to bring about the whole folding process. This is supported by the fact that neutral detergents are generally able to induce the folding of hydrophobic transmembrane peptides, whereas they are not able to fold the hydophilic peptides used in this study. Consequently, any mechanism for SDS-induced helix formation should take into account the characteristics of the peptide characters, including (i) the presence of positively charged residues favoring SDS anchoring via salt bridge formation, (ii) the presence of large hydrophobic residues which will favor SDS binding via its aliphatic tail, and (iii) the presence of a number of negatively charged residues which, by electrostatic repulsion, can prevent SDS binding.

ACKNOWLEDGMENT

Thanks are due to D. Ficheux from IBCP for peptide synthesis and purification. This work is dedicated to the memory of Xavier Rafaitin who died in an avalanche at the age of 24.

REFERENCES

1. Dong, M., Penin, F., and Baggetto, L. G. (1996) *J. Biol. Chem. 271*, 28875−28883.
2. Dong, M., Baggetto, L. G., Falson, P., Le Maire, M., and Penin, F. (1997) *Anal. Biochem. 247*, 333−341.
3. Reynolds, J. A., and Tanford, C. (1970) *J. Biol. Chem. 245*, 5161−5165.
4. Mattice, W. L., Riser, J. M., and Clark, D. S. (1976) *Biochemistry 15*, 4264−4272.
5. Wu, C.-S. C., and Yang, J. T. (1978) *Biochem. Biophys. Res. Commun. 82*, 85−91.
6. Pervushin, K. V., Orekhov, V. Yu., Popov, A. I., Musina, L. Yu., and Arseniev, A. S. (1994) *Eur. J. Biochem. 219*, 571−583.
7. Chang, D. K., Cheng, S. F., and Chien, W. J. (1997) *J. Virol. 71*, 6593−6602.
8. Papavoine, C. H., Konings, R. N., Hilbers, C. W., and Van de Ven, F. J. (1994) *Biochemistry 33*, 12990−12997.
9. Chupin, V., Killian, J. A., Breg, J., de Jongh, H. H., Boelens, R., Kaptein, R., and de Kruijff, B. (1995) *Biochemistry 34*, 11617−11624.
10. van den Hooven, H. W., Doeland, C. C., Van De Kamp, M., Konings, R. N., Hilbers, C. W., and Van De Ven, F. J. (1996) *Eur. J. Biochem. 235*, 382−393.
11. Young, J. K., Mari, F., Xu, M., Humphreys, R. E., Clemente, N. M., Stattel, J. M., Nelson, D. J., Gambino, J., and Wright, G. E. (1997) *J. Pept. Res. 50*, 122−131.
12. McLeish, M. J., Nielsen, K. J., Wade, J. D., and Craik, D. J. (1993) *FEBS Lett. 315*, 323−328.
13. McLeish, M. J., Nielsen, K. J., Najbar, L. V., Wade, J. D., Lin, F., Doughty, M. B., and Craik, D. J. (1994) *Biochemistry 33*, 11174−11183.
14. Najbar, L. V., Craik, D. J., Wade, J. D., Lin, F., and McLeish, M. J. (1995) *Biochim. Biophys. Acta 1250*, 163−170.
15. Najbar, L. V., Craik, D. J., Wade, J. D., Salvatore, D., and McLeish, M. J. (1997) *Biochemistry 36*, 11525−11533.
16. Montserret, R., Aubert-Foucher, E., McLeish, M. J., Hill, J. M., Ficheux, D., Jaquinod, M., van der Rest, M., Deléage, G., and Penin, F. (1999) *Biochemistry 38*, 6479−6488.
17. Buck, M. (1998) *Q. Rev. Biophys. 31*, 297−355.
18. Mammi, S., and Peggion, E. (1990) *Biochemistry 29*, 5265−5269.
19. Rizo, J., Blanco, F. J., Kobe, B., Bruch, M. D., and Gierasch, L. M. (1993) *Biochemistry 32*, 4881−4894.
20. Zhong, L., and Johnson, W. C., Jr. (1992) *Proc. Natl. Acad. Sci. U.S.A. 89*, 4462−4465.
21. Waterhous, D. V., and Johnson, W. C. (1994) *Biochemistry 33*, 2121−2128.
22. Brito, R. M., and Vaz, W. L. (1986) *Anal. Biochem. 152*, 250−255.
23. Wu, C.-S. C., Ikeda, K., and Yang, J. T. (1981) *Biochemistry 20*, 566−570.
24. Yonath, A., Podjarny, A., Honig, B., Sielecki, A., and Traub, W. (1977) *Biochemistry 16*, 1418−1424.
25. Cardin, A. D., Demeter, D. A., Weintraub, H. J. R., and Jackson, R. L. (1991) *Methods Enzymol. 203*, 556−583.
26. Ferran, D. S., Sobel, M., and Harris, R. B. (1992) *Biochemistry 31*, 5010−5016.
27. Giry-Lozinguez, C., Aubert-Foucher, E., Penin, F., Deléage, G., Dublet, B., and van der Rest, M. (1998) *Matrix Biol. 17*, 145−149.
28. Marcinowski, K. J., Shao, H., Clancy, E. L., and Zagorski, M. G. (1998) *J. Am. Chem. Soc. 120*, 11082−11091.

29. Deuel, T. F., Keim, P. S., Farmer, M., and Heinrikson, R. L. (1977) *Proc. Natl. Acad. Sci. U.S.A. 74*, 2256−2258.
30. Zhang, X., Chen, L., Bancroft, D. P., Lai, C. K., and Maione, T. E. (1994) *Biochemistry 33*, 8361−8366.
31. Woody, R. W. (1985) Circular dichroism of peptides, in *The Peptides* (Udenfried, S., Meienhofer, J., and Hruby, V. J., Eds.) Vol. 7, pp 15−114, Academic Press, New York.
32. Chen, Y.-H., Yang, J. T., and Chau, K. H. (1974) *Biochemistry 13*, 3350−3359.
33. Lesage, A., Penin, F., Geourjon, C., Marion, D., and van der Rest, M. (1996) *Biochemistry 35*, 9647−9660.
34. Penin, F., Geourjon, C., Montserret, R., Böckmann, A., Lesage, A., Yang, Y. S., Bonod-Bidaud, C., Cortay, J. C., Nègre, D., Cozzone, A. J., and Deléage, G. (1997) *J. Mol. Biol. 270*, 496−510.
35. Wüthrich, K. (1986) in *NMR of proteins and nucleic acids*, John Wiley and Sons, New York.
36. Brünger, A. T. (1992) in *Xplor, a system for crystallography and NMR*, Yale University Press, New Haven, CT.
37. Geourjon, C., and Deléage, G. (1995) *J. Mol. Graphics 13*, 209−212.
38. Sayle, R. A., and Milner-White, E. J. (1995) *Trends Biochem. Sci. 20*, 374.
39. Laskowski, R. A., Rullmannn, J. A., MacArthur, M. W., Kaptein, R., and Thornton, J. M. (1996) *J. Biomol. NMR 8*, 477−486.
40. Ilyina, E., Milius, R., and Mayo, K. H. (1994) *Biochemistry 33*, 13436−13444.
41. Eisenberg, D., Weiss, R. M., and Terwilliger, T. C. (1982) *Nature 299*, 371−374.
42. Chou, P. Y., and Fasman, G. D. (1978) *Adv. Enzymol. 47*, 45−148.
43. Zhou, N. E., Kay, C. M., Sykes, B. D., and Hodges, R. S. (1993) *Biochemistry 32*, 6190−6197.
44. Jasanoff, A., and Fersht, A. R. (1994) *Biochemistry 33*, 2129−2135.
45. Tessari, M., Foffani, M. T., Mammi, S., and Peggion, E. (1993) *Biopolymers 33*, 1877−1887.
46. Wishart, D. S., Bigam, C. G., Yao, J., Abildgaard, F., Dyson, H. J., Oldfield, E., Markley, J. L., and Sykes, B. D. (1995) *J. Biomol. NMR 6*, 135−140.
47. Böckmann, A., and Guittet, E. (1996) *J. Biomol. NMR 8*, 87−92.
48. Wang, G., Treleaven, W. D., and Cushley, R. J. (1996) *Biochim. Biophys. Acta 1301*, 174−184.
49. Wu, C.-S. C., and Yang, J. T. (1988) *Biopolymers 27*, 423−430.
50. Dill, K. A., and Shortle, D. (1991) *Annu. Rev. Biochem. 60*, 795−825.
51. Dyson, H. J., and Wright, P. E. (1991) *Annu. Rev. Biophys. Biophys. Chem. 20*, 519−538.
52. Kraulis, P. J. (1991) *J. Appl. Crystallogr. 24*, 946−950.
53. Merritt, E. A., and Murphy, M. E. P. (1994) *Acta Crystallogr., Sect. D 50*, 869−873.

BI000208X